

# WIRELESS FRACTAL CELLULAR NETWORKS

XIAOHU GE, YEHONG QIU, JIAQI CHEN, MEIDONG HUANG, HUI XU, JING XU, WUXIONG ZHANG, YANG YANG, CHENG-XIANG WANG, AND JOHN THOMPSON

## ABSTRACT

With the seamless coverage of wireless cellular networks in modern society, it is interesting to consider the shape of wireless cellular coverage. Is the shape a regular hexagon, an irregular polygon, or another complex geometrical shape? Based on fractal theory, the statistical characteristic of the wireless cellular coverage boundary is determined by the measured wireless cellular data collected from Shanghai, China. The measured results indicate that the wireless cellular coverage boundary presents an extremely irregular geometrical shape, which is also called a statistical fractal shape. Moreover, the statistical fractal characteristics of the wireless cellular coverage boundary have been validated by values of the Hurst parameter estimated in angular scales. The statistical fractal characteristics of the wireless cellular coverage boundary can be used to evaluate and design the handoff scheme of mobile user terminals in wireless cellular networks.

## INTRODUCTION

It is estimated that 90 percent of the world's population over 6 years old will have a mobile phone by 2020, that is, most of the population will be covered by wireless cellular networks [1]. The coverage shape of a wireless cell is formed by the wireless cellular coverage boundary, which is connected by all of the farthest locations around a base station (BS). The farthest locations are also called wireless cellular coverage boundary points, where the received wireless signal power is equal to the minimum power threshold  $P_{min}$  configured by the cellular network. An important challenge for wireless cellular network providers is to ensure that mobile users are seamlessly covered by adjacent BSs, especially those located at the edge of wireless cells [2]. Moreover, the user handoff between adjacent wireless cell signals depends on the wireless cellular coverage boundary in wireless cellular networks. Therefore, the shape of the wireless cellular coverage boundary is a critical metric for the design, deployment, and optimization of wireless cellular networks.

Wireless cellular coverage shapes have been investigated for wireless cellular networks over the past few decades [3, 4]. Assuming that the propagation environment is free space and that the BS wireless signal is uniformly radiated in all directions, the wireless cellular coverage shape should be a circle with the BS located at

the center in a two-dimensional plane [3]. When BSs are assumed to be uniformly deployed with equal distances in a wireless cellular network, the wireless cellular network service region can be split into multiple regular triangles, squares, or regular hexagons that seamlessly cover the service region without overlaps. Considering that a regular hexagon is the closest to a circle among all candidate shapes (i.e., regular triangle, square, and regular hexagon), a regular hexagon has been widely adopted as the wireless cellular coverage model in conventional wireless cellular networks [3]. With an increase in the density of BSs, existing studies have indicated that the performance of regular hexagon wireless cellular networks deviates from the performance of real wireless cellular networks [4]. Based on measured data, the locations of BSs can be approximated by a Poisson point process distribution for wireless cellular networks [4]. Moreover, the wireless cell boundaries, which are obtained through the Delaunay triangulation method by connecting the perpendicular bisector lines between each pair of BSs, split the wireless cellular network service region into multiple irregular polygons that correspond to different wireless cellular coverage areas. This stochastic and irregular topology creates the need for a so-called Poisson-Voronoi tessellation (PVT) method [3]. However, the impact of wireless signal propagation environments on the wireless cell boundary is not considered in the PVT random wireless cellular network models. Moreover, to simplify system models, the path loss fading of a wireless signal in the PVT network model is assumed to be equal in all directions if the distances between receivers and the BS are equal. This assumption ignores the anisotropy of path loss fading in real wireless signal propagation environments. Moreover, conventional geometric segmentation methods used to form wireless cell boundaries, such as the PVT method, result in a smooth wireless cell boundary at small scales. However, the measured cellular data indicates that the PVT method cannot provide an accurate estimation of real wireless cellular coverage shapes [5].

The wireless cellular coverage boundary is not smooth at small scales because the wireless signal fading in real environments is affected by electromagnetic radiation, the atmospheric environment, weather status, obstacle distribution, and diffraction and scattering effects in different propagation directions. Considering the irregular

Xiaohu Ge, Yehong Qiu, Jiaqi Chen, and Meidong Huang are with Huazhong University of Science and Technology.

Hui Xu, Jing Xu, Wuxiong Zhang, and Yang Yang are with the Chinese Academy of Sciences.

Cheng-Xiang Wang is with Heriot-Watt University.

John Thompson is with the University of Edinburgh.

Measurement environment	GPS location of BS	Transmission power	Feeder loss at the antenna	Antenna transmission gain (Tx)	Antenna receive gain (Rx)
Pingjiang Road, Shanghai, China	Latitude = 31.202252 Longitude = 121.451055	38 dBm	0.5 dB	12 dBi	3 dBi

Table 1. Base station configuration.

distribution of buildings in urban environments, electromagnetic waves are absorbed, reflected, scattered, and diffracted in different directions. Therefore, in urban environments, wireless signals transmitted by BSs undergo different amounts of attenuation and fading in different directions before arriving at the users. The existing study in [6] validated that the probability density function (PDF) of the interference exhibits a heavy-tailed characteristic. Moreover, the traffic load of cellular networks has been demonstrated to manifest the self-similar characteristic, which is also conducive to the heavy-tailed distribution of traffic load [7]. Essentially, several effects such as wireless signal attenuation, network traffic, and the interference caused by adjacent BSs may affect the shape of the wireless cellular coverage boundary. As a consequence, wireless cellular coverage boundaries present extremely irregular shapes at small scales for real wireless cellular networks. However, it is difficult to describe extremely irregular wireless cell boundaries using conventional Euclidean geometry methods.

As an important extension of the conventional Euclidean geometry theory, fractal geometry theory describes geometric shapes between extreme geometric orders and full chaos [8]. Based on the measured wireless cellular data, we utilize the typical wireless signal propagation model and the least squares method to estimate the path loss coefficient and shadow fading. In this case, real wireless signal propagation environments are focused, and other potential roots, such as the network traffic and the interference resulting in heavy-tailed characteristic of wireless cellular coverage boundary, are ignored in this study. We report that the real wireless cellular coverage boundary is a non-smooth boundary in urban environments. Furthermore, utilizing fractal geometry theory, the real wireless cellular coverage boundary has statistical fractal characteristics at angular scales, and real wireless signal propagation environments are conducive to statistical fractal characteristics of the wireless cellular coverage boundary in angular scales. The statistical fractal is not an exact fractal that can be denoted by an exact fractal expression [9]. Compared to an exact fractal, the statistical fractal is more suitable for describing geometric shapes in the real world. The quantization of a statistical fractal is typically estimated by the value of the Hurst parameter [10]. Three typical statistical estimators, that is, the periodogram method, the rescaled adjusted range statistic (R/S) method, and the variance-time analysis method, are utilized to estimate the value of the Hurst parameter for real wireless cellular coverage boundaries. The estimated results indicate that the real wireless cellular coverage boundary has the statistical fractal characteristic at angular scales. Oppositely, a comparison of the results

demonstrates that a mathematically derived wireless cellular coverage boundary does not have statistical fractal characteristics at angular scales. Although the experimental measurement in this article is carried out in cellular networks, the analysis results reflect the coverage characteristic of wireless communications considering wireless signal propagation environments. Therefore, our results can also be used for other wireless communication scenarios, such as WLANs.

## MEASURED AND DERIVED WIRELESS CELLULAR COVERAGE SHAPES

The wireless signal power received at a mobile user terminal is measured by a continuous wave test signal method that is widely used to evaluate wireless propagation environments [11]. The measurement solution in this article is configured as follows. A BS equipped with an omnidirectional antenna is located at Pingjiang Road, Shanghai, China. The BS transmits wireless signals at a fixed frequency of 2.6 GHz and a fixed transmission power of 38 dBm. The detailed BS configuration parameters are shown in Table 1. The received wireless signal power is measured by a mobile user terminal equipped with an omnidirectional antenna that moves along a specified route, as shown in Fig. 1. The measurement data was collected on May 15, 2014. The specified route passes through office buildings, residential houses, and green belts in Shanghai. The mobile user terminal moved around the cellular coverage region to measure the received wireless signal power and the corresponding global positioning system (GPS) data, which facilitated the estimation of the distance between the mobile user terminal and the BS.

In wireless communications, wireless signal fading is typically classified in two parts: large-scale fading, which includes path loss fading and shadow fading, and small-scale fading, which includes multipath fading. In practical wireless signal measurement applications, the received wireless signal power is averaged over several wavelengths to eliminate the multipath fading effect [12]. In our wireless signal measurements, the wireless signal power is averaged over 40 wavelengths by a mobile user terminal. In this case, the small-scale fading is ignored due to the averaged multipath fading effect [11]. Moreover, the path loss fading is denoted as  $d^{-\gamma}$ , where  $\gamma$  is the path loss coefficient and  $d$  is the distance between a receiver and a BS. The shadow fading is denoted as  $\psi$ . For the derived wireless cellular coverage regions, the path loss fading is assumed to be equal in all directions of the derived wireless cellular coverage regions when the distance between a receiver and a BS is the same. Based on the measured wireless cellular data, the average path loss coefficient  $\gamma$  is estimated using the

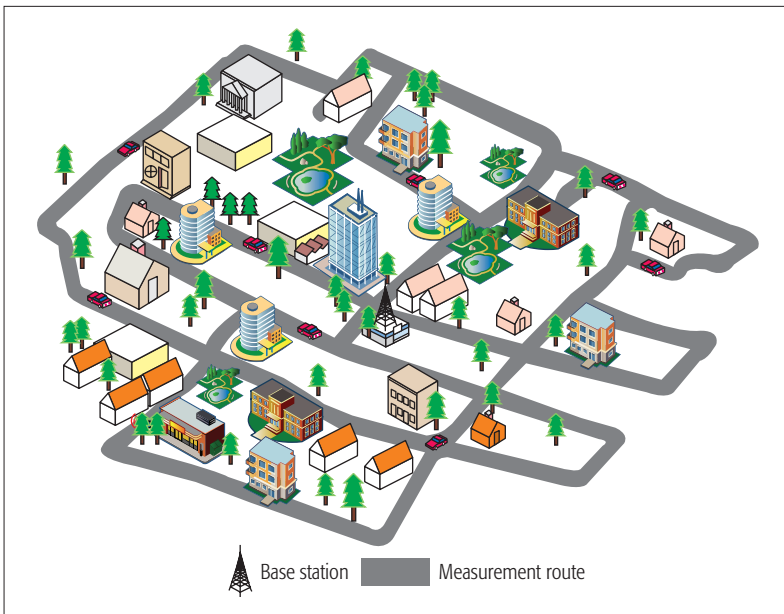


Figure 1. BS location and measurement route. The BS location is denoted by a BS icon, and the grey line is the measurement.

least squares method. In addition, the shadow fading is assumed to follow a log-normal distribution [13]. Without loss of generality, the shadow fading is assumed to follow a log-normal distribution with a mean of  $\mu = 0$  dB and a standard deviation of  $\sigma = 4$  dB for the mathematically derived wireless cellular coverage regions [14]. However, for real wireless cellular coverage regions, the path loss fading and shadow fading are not the same in different propagation directions and depend on real propagation paths.

In Fig. 2a, the transmission wireless signal power presents a power peak at the BS location and then uniformly attenuates in all propagation directions with increasing distance. Moreover, the transmission wireless signal power varies smoothly with increasing distance, especially at locations far away from the BS. When the minimum received wireless signal power threshold is configured as  $P_r = -110$  dBm, the corresponding equal power curve at  $-110$  dBm of the received wireless signal is plotted to form the derived wireless cellular coverage region, as shown in Fig. 2b. The derived wireless cellular coverage boundary appears as an amoeba around the BS.

Considering the non-uniform distribution of different sizes of office buildings and large obstacles in real propagation paths, the path loss fading should present anisotropy in different propagation directions in urban environments. In other words, the path loss fading values at different locations are different even though these locations have the same distance to the BS in real wireless propagation environments. Furthermore, the path loss coefficient is not a constant in different propagation directions and depends on real propagation paths. In Figs. 2c and 2d, the path loss coefficients of different directions are estimated using the measured wireless cellular data in corresponding directions. Moreover, the shadow fading is estimated using a least squares method for measured wireless cellular coverage regions. Figure 2c shows the transmission wire-

less signal power measured from real propagation environments. In Fig. 2c, the transmission wireless signal power presents a power peak at the BS location and then non-uniformly attenuates in different propagation directions with increasing distance. Clear phenomena can be observed, with a “mountain top” and a “mountain valley” around the power peak, as shown in Fig. 2c. This result implies that the path loss fading exhibits the expected anisotropy in different propagation directions. When the minimum received wireless signal power threshold is configured as  $P_r = -110$  dBm, the corresponding received wireless signal equal power curve with  $-110$  dBm is plotted to form the measured wireless cellular coverage region, as shown in Fig. 2d. The measured wireless cellular coverage boundary does not have the appearance of an amoeba around the BS and presents extreme irregularity at small scales. Therefore, it is difficult to describe the real wireless cellular boundary using conventional Euclidean geometry methods.

## MEASURED AND DERIVED WIRELESS CELLULAR COVERAGE BOUNDARIES

To quantitatively analyze the irregularity of wireless cellular coverage boundaries, the received wireless signal equal power line is discretized for evaluating the geometry characteristics in small scales. To obtain discrete wireless cellular coverage boundary points, the measured wireless cellular coverage region is partitioned into 120 sections centered at the BS and  $3^\circ$  angular width. Moreover, the path loss coefficient is assumed to be identical in a section propagation environment when the section angle is sufficiently small, such as when the section angle is less than or equal to  $3^\circ$ . Based on the testing route circling around the BS, testing points are obtained and distributed in the same section with different distances from the BS. Compared with a mix of non-line-of-sight (NLOS) and line-of-sight (LOS) path loss models, a general path loss model would be an average of the path loss coefficient in the corresponding section. Moreover, the general path loss model does not change the relationship with other sections in a cell. Hence, a general path loss model is adopted in this study by  $P_{rd} = P_{rd_0} - 10\gamma\log_{10}(d/d_0) - \psi$  [3], where  $P_{rd}$  is the measured received wireless signal power at a mobile user terminal with distance from the BS  $d$ ,  $P_{rd_0}$  is the measured received wireless signal power at a reference location with distance from the BS  $d_0$ , and  $\gamma$  and  $\psi$  are the path loss coefficient and shadow fading, respectively. Based on the wireless signal propagation model and measured received wireless signal power of testing points in the  $k$ th section, the path loss coefficient  $\gamma_k$  and shadow fading  $\psi_k$  are estimated by a least squares method for the  $k$ th section of the measured wireless cellular coverage region. For details, the values of  $(P_{rd_0} - P_{rd})$  vs.  $10\log_{10}(d/d_0)$  are first plotted in a Euclidean coordinate system. The wireless signal propagation model is fitted by a least squares line formed by measured data collected from the  $k$ th section. As a result, the asymptotic slope of the least squares fits the path loss coefficient  $\gamma_k$  and the asymptotic intercept is the shadow fading  $\psi_k$  in the  $k$ th section of

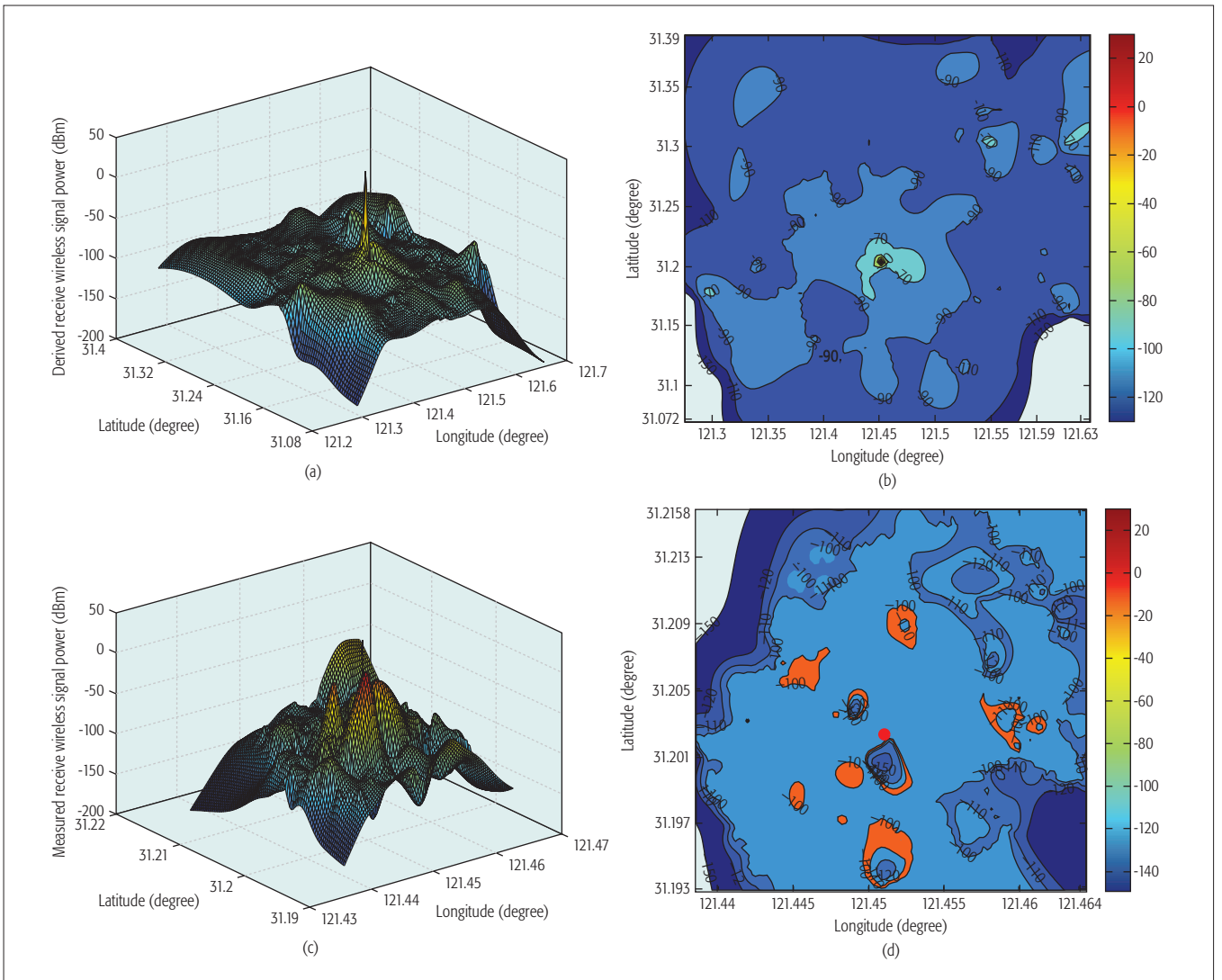


**Figure 2.** Derived and measured received wireless signal power figures. The bright red regions denote the highest received wireless signal power, and the ultramarine regions denote the lowest received wireless signal power. The received wireless signal power decreases with the color changing from bright red to ultramarine: a) received wireless signal power level based on the derived wireless cellular coverage; b) received wireless signal equal power curve based on the derived wireless cellular coverage. The black line is the received equal power liner level; the same color region indicates that the value of the wireless signal power is between two power values denoted by two black lines; c) received wireless signal power level based on the measured wireless cellular coverage; d) received wireless signal equal power curve based on the measured wireless cellular coverage. The black line is the received equal power liner level, and the same color region indicates that the value of wireless signal power is between two power values denoted by two black lines.

the measured wireless cellular coverage region. When the received wireless signal power threshold at the wireless cellular coverage boundary is configured as  $P_{r\phi} = P_{min} = -110$  dBm and the reference location  $d_0$  is configured as the  $i$ th testing point in the  $k$ th section, the distance  $\phi_{k,i}$  between the discrete boundary point and the BS is calculated by the wireless signal propagation model based on the estimated path loss coefficient  $\gamma_k$  and shadow fading  $\psi_k$  in the  $k$ th section of the measured wireless cellular coverage region. When all sections of the wireless cellular coverage region are measured, the distance series  $\phi$  of the measured wireless cellular coverage boundary is obtained for further statistical analysis. The measured wireless cellular coverage boundary is plotted in Fig. 3a when all discrete boundary points are connected. The average

path loss coefficient is calculated by the total measured wireless cellular data for the derived wireless cellular coverage region. Moreover, the average path loss coefficient is used for every section in the derived wireless cellular coverage region, and the shadow fading is estimated by a log-normal distribution. Furthermore, a discrete boundary point is derived by the wireless channel propagation model for a section in the derived wireless cellular coverage region. The derived wireless cellular coverage boundary is plotted in Fig. 3b when all discrete boundary points are connected. Comparing Figs. 3a and 3b, the measured wireless cellular coverage boundary presents a large-scale fluctuation (i.e., a bursty characteristic), while the derived wireless cellular coverage boundary is a smooth circle.

To analyze the statistical characteristic of the

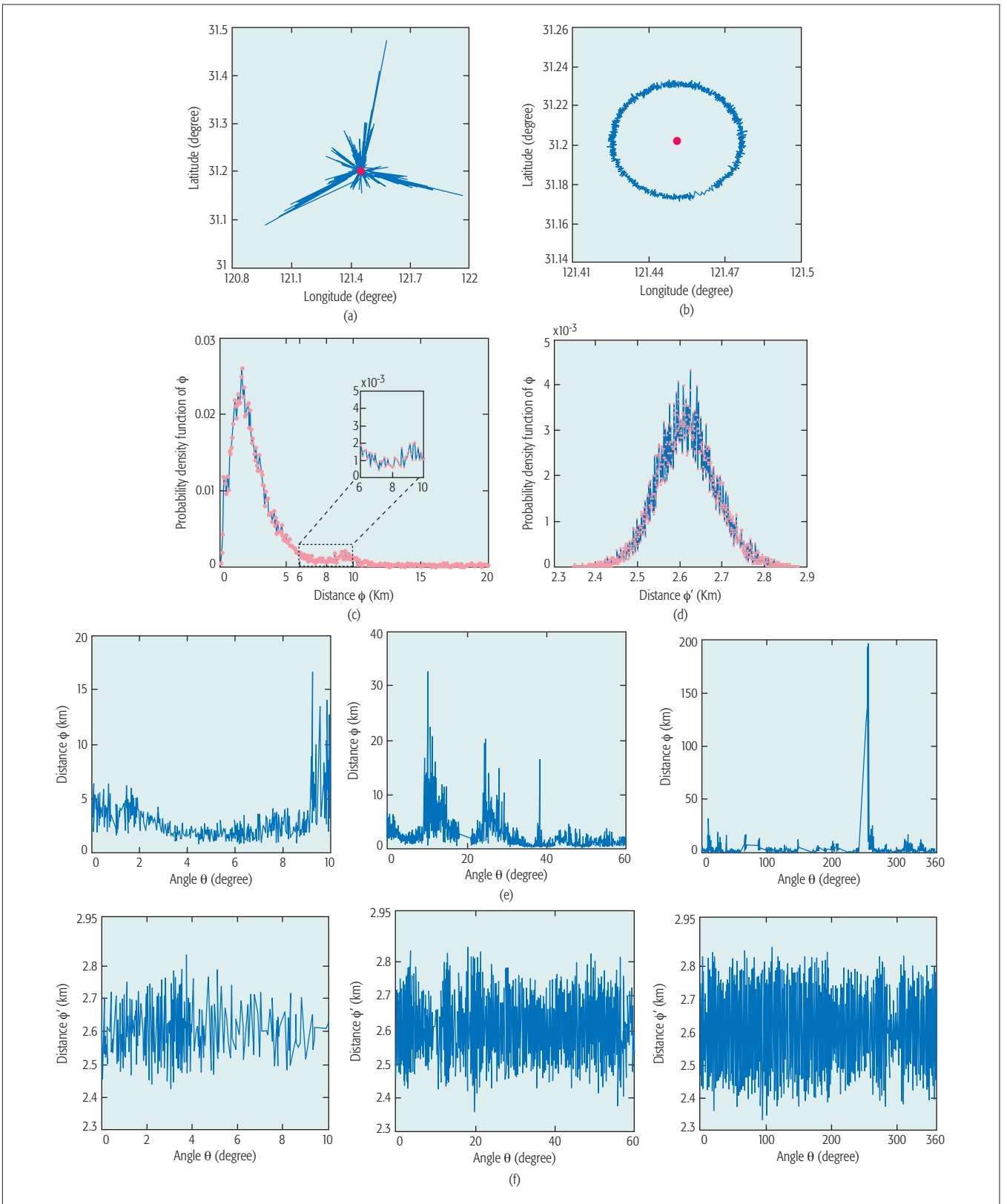


**Figure 3.** Measured and derived wireless cellular coverage boundaries: a) measured wireless cellular coverage shape; the red point is the BS, and the blue curve is the measured wireless cellular coverage boundary; b) derived wireless cellular coverage shape; the red point is the BS, and the blue curve is the derived wireless cellular coverage boundary; c) PDF of the distance  $\phi$ , where the pink points are the statistical probability points generated from the measured wireless cellular coverage boundary and the blue curve is the contact line in discrete statistical probability points; d) PDF of the distances  $\phi'$ , where the pink points are the statistical probability points generated from the derived wireless cellular coverage boundary and the blue curve is the contact line in discrete statistical probability points; e) distances  $\phi$  between the discrete boundary point and BS with respect to the angle  $\theta$  in the measured wireless cellular coverage boundary; f) distances  $\phi'$  between the discrete boundary point and BS with respect to the angle  $\theta$  in the derived wireless cellular coverage boundary.

wireless cellular coverage boundary, let  $\phi$  and  $\phi'$  be the distances between the BS and a discrete boundary point in the measured wireless cellular coverage boundary and derived wireless cellular coverage boundary, respectively. Figures 3c and 3d are the PDF of the distances  $\phi$  and  $\phi'$ , respectively. Based on results in Fig. 3d, the shape of the PDF of the distance  $\phi'$  is a typical shape of a Gaussian distribution. Compared to the shape in Fig. 3d, the shape of the PDF of the distance  $\phi$  presents a heavy-tailed characteristic in Fig. 3c. The heavy-tailed characteristic of the PDF of the distance  $\phi$  implies that some small probability events, such as some discrete boundary points that are far away from the BS, cannot be ignored in forming the distribution of a measured wireless cellular coverage boundary. Hence, the distribution of a measured wireless cellular coverage boundary is a non-Gaussian distribution.

Considering the heavy-tailed and bursty characteristics in the analysis of the measured wireless cellular coverage boundary, we investigate the measured wireless cellular coverage boundary using fractal theory. Unlike conventional fractal studies at temporal scales and spatial scales [15], the fractal study of the measured wireless cellular coverage boundary is analyzed in angular scales in this article. Without loss of generality, an angle denoted as  $\theta$  is between the east direction line and a given line that is crossed with a discrete boundary point and the BS. Figure 3e illustrates distances  $\phi$  between discrete boundary points and the BS with respect to the angle  $\theta$  for the measured wireless cellular coverage boundary. The peak range of the distance for the measured wireless cellular coverage boundary exhibits burstiness when the angle is restricted by  $0^\circ \sim 10^\circ$ . When the angle  $\theta$  is extended from  $0^\circ \sim 10^\circ$  to  $0^\circ \sim 60^\circ$ , that is, the angle scale is zoomed in six times, the distance  $\phi$  clearly exhibits burstiness, and the peak value of the distance is 34 km. When the angle  $\theta$  is extended from  $0^\circ \sim 60^\circ$  to  $0^\circ \sim 360^\circ$ , that is, the angle scale is zoomed in six times again, the distance  $\phi$  still exhibits clear burstiness, and the peak value of the distance is 200 km. Figure 3e shows that the burstiness of distances at different angular scales of the measured wireless cellular coverage boundary cannot be smoothed by zooming in to angular scales, that is, there is always burstiness of the distances at all angular scales of the measured wireless cellular coverage boundary. This phenomenon is called a fractal or self-similarity phenomenon in angular scales [16]. Figure 3f illustrates distances  $\phi'$  between the discrete boundary points and BS with respect to the angle  $\theta$  for the derived wireless cellular coverage boundary. The peak range of the distance exhibits burstiness for the derived wireless cellular coverage boundary when the angle is restricted to the range of  $0^\circ \sim 10^\circ$ . When the angle  $\theta$  is extended from  $0^\circ \sim 10^\circ$  to  $0^\circ \sim 60^\circ$ , that is, the angular scale is zoomed in six times, the peak range of the distance  $\phi'$  is nearly smooth. When the angle  $\theta$  is extended from  $0^\circ \sim 60^\circ$  to  $0^\circ \sim 360^\circ$ , that is, the angular scale is zoomed in six times again, the peak range of the distance  $\phi'$  is fully smooth. Figure 3f indicates that the burstiness of distances at small angular scales

can be smoothed with increases in the angular scales in the derived wireless cellular coverage boundary. Hence, there is no fractal or self-similarity phenomenon in the angular scales for the mathematically derived wireless cellular coverage boundary.

## FRACTAL EVALUATION OF THE MEASURED WIRELESS CELLULAR COVERAGE BOUNDARY

No exact fractal phenomenon exists in the real world. Most of the fractal phenomena observed in the real world only have the statistical fractal characteristic [6, 7]. Statistical fractal random processes present the spectral density power-law behavior and the slowly decaying variance characteristic in the frequency and time domains, respectively. Moreover, the statistical fractal characteristic of random processes is evaluated by the Hurst parameter, which can be estimated using three typical methods [17].

**The Periodogram Method:** This method plots the logarithm of the spectral density of a series vs. the logarithm of frequencies. The Hurst parameter can be estimated by  $H = (1/2)(1 + \alpha)$  where  $\alpha$  is the slope in the log-log plot. The series has a statistical fractal character if  $\{0.5 < H < 1\}$ .

**The Rescaled Adjusted Range Statistic (R/S) Method:** For a random process  $X_i$ , the partial sum is denoted by

$$Y(n) = \sum_{i=1}^n X_i,$$

and sample variance is denoted by

$$S^2(n) = \frac{\sum_{i=1}^n X_i - \frac{Y(n)}{n}}{n}, \quad n \geq 1.$$

Furthermore, the R/S statistic is defined as

$$\frac{R(n)}{S(n)} = \frac{\max_{0 \leq t \leq n} 0, Y(t) - \frac{t}{n} Y(n) - \min_{0 \leq t \leq n} 0, Y(t) - \frac{t}{n} Y(n)}{s(n)}, \quad n \geq 1.$$

A log-log plot of the R/S statistic vs. the number of points of the aggregated series should be a straight line with the slope being an estimation of the Hurst parameter. The random process  $X_i$  is statistical fractal if the value of the Hurst parameter  $H$  is in the interval (0.5, 1.0).

**The Variance-Time Analysis Method:** This involves the definition of an aggregated series  $X^{(m)}$ , using different block sizes  $m$ . The log-log plot of the sample variance vs. the aggregation level should be a straight line with the slope  $\beta$  in the interval (0, 1) if the data are statistical fractal. In this case,  $H = 1 - (\beta/2)$ .

Let  $X = \{\phi_i, i = 1, 2, \dots, N\}$  and  $X' = \{\phi'_i, i = 1, 2, \dots, M\}$  be two independent random processes, where  $N$  and  $M$  are the number of discrete measured and derived wireless cellular coverage boundary points, and  $\phi_i$  and  $\phi'_i$  are the distances between the  $i$ th discrete boundary point and the

Statistical fractal random processes present the spectral density power-law behavior and the slowly decaying variance characteristic in the frequency and time domains, respectively. Moreover, the statistical fractal characteristic of random processes is evaluated by the Hurst parameter, which can be estimated using three typical methods.

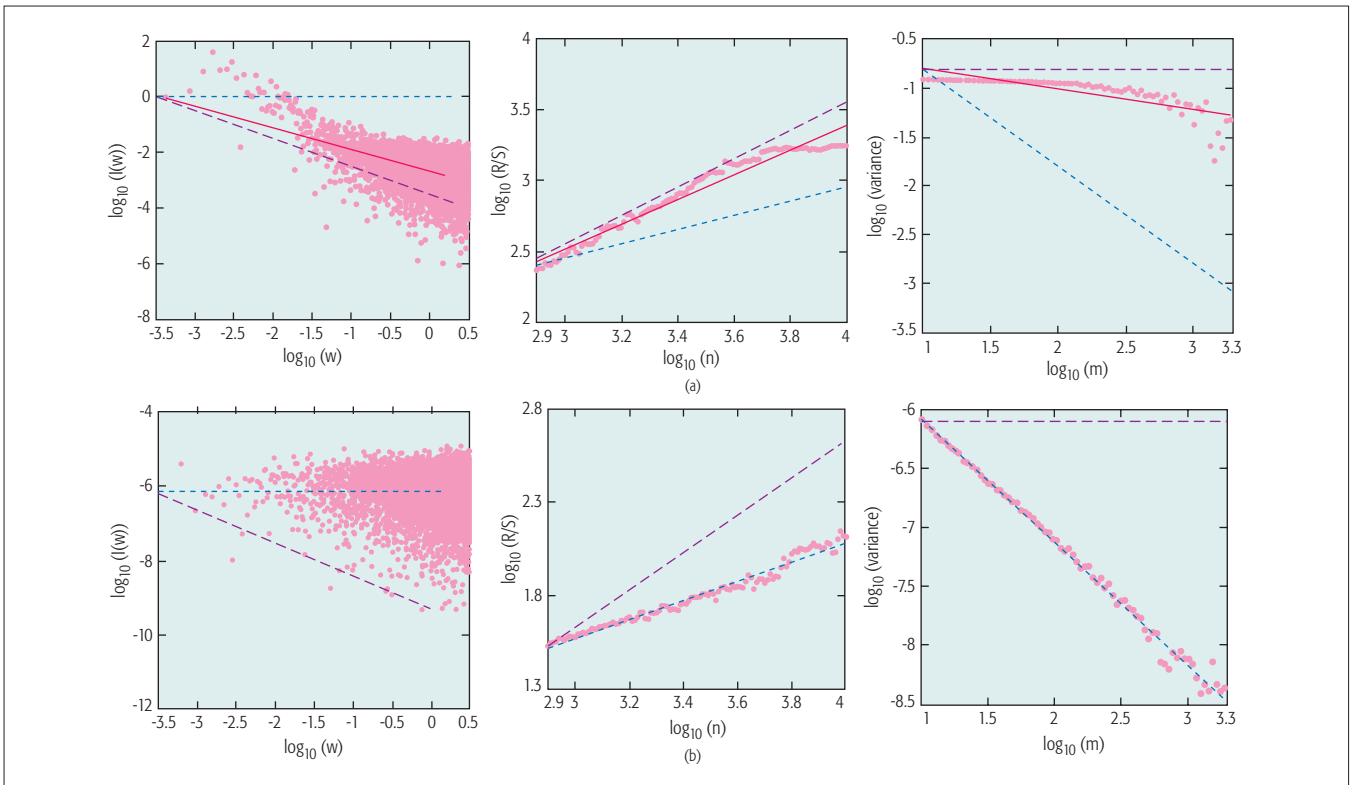


**Figure 4.** Statistical fractal of the measured and derived wireless cellular coverage boundaries: a) statistical fractal estimation of the measured wireless cellular coverage boundary; the red line is the fitted line based on the measured wireless cellular coverage boundary data, where the value of the Hurst parameter is  $H \approx 0.9$ , the blue broken line corresponds to the value of the Hurst parameter  $H = 0.5$ , and the purple broken line corresponds the value of Hurst parameter  $H = 1$ ; b) statistical fractal estimation of the derived wireless cellular coverage boundary; the blue broken line is the fitted line based on the derived wireless cellular coverage boundary data where the value of the Hurst parameter is  $H = 0.5$ , and the purple broken line corresponds to the value of the Hurst parameter  $H = 1$ .

BS in the measured wireless cellular coverage boundary and derived wireless cellular coverage boundary, respectively. Figure 4a illustrates the values of the Hurst parameter estimated from the measured wireless cellular coverage boundary data using the periodogram method, R/S method, and variance-time analysis method. On the left of Fig. 4a, the periodogram method is used to estimate the value of the Hurst parameter based on the spectral density  $I(w)$  of the random process  $X = \{\phi_i, i = 1, 2, \dots, N\}$  in a log-log plot. When the frequency value  $w$  approaches zero, the spectral density presents a low-power decaying behavior in the log-log plot. Utilizing a least squares method, the slope, that is, the decay rate of the spectral density in the log-log plot, is estimated as  $\alpha = 0.8026$ . Furthermore, the value of the Hurst parameter is calculated by  $H = (1/2)(1 + \alpha) = 0.9013$ . In the middle of Fig. 4a, the R/S method is used to estimate the value of the Hurst parameter by the R/S statistic of the random process  $X = \{\phi_i, i = 1, 2, \dots, N\}$  in a log-log plot. The R/S statistic increases linearly with increases in the length of series  $n$  in a log-log plot. Utilizing a least squares method, the Hurst parameter (i.e., the slope in the log-log plot) is estimated as  $H = 0.8898$ . On the right of Fig. 4a, the variance-time analysis method is used to estimate the value of the Hurst parameter by the variance of the aggregated series of the random process  $X = \{\phi_i, i = 1, 2, \dots, N\}$  in a log-log plot. The variance of the aggregated series presents a

slow decaying characteristic with increases in the aggregation level  $m$  in a log-log plot. Utilizing a least squares method, the slope of the sample variance is estimated as  $\beta = 0.2000$  in the log-log plot. Furthermore, the value of the Hurst parameter is calculated to be  $H = 1 - (\beta/2) = 0.9000$ . Based on the results from the three Hurst parameter estimators, the value of the Hurst parameter estimated from the measured wireless cellular coverage boundary is clearly larger than 0.5 and is approximately  $H \approx 0.9$ .

Figure 4b illustrates the Hurst parameter estimated from the derived wireless cellular coverage boundary data by the periodogram method, R/S method, and variance-time analysis method. On the left of Fig. 4b, the periodogram method is used to estimate the value of the Hurst parameter by the spectral density of the random process  $X' = \{\phi'_i, i = 1, 2, \dots, M\}$  in a log-log plot. When the frequency value approaches zero, the spectral density remains nearly constant in the log-log plot. Utilizing the least squares method, the slope, that is, the decay speed of spectral density in the log-log plot, is estimated to be  $\alpha = 0.001$ . Furthermore, the value of the Hurst parameter is calculated to be  $H = (1/2)(1 + \alpha) = 0.4995 \approx 0.5$ . In the middle of Fig. 4b, the R/S method is used to estimate the value of the Hurst parameter based on the R/S statistic of the random process  $X' = \{\phi'_i, i = 1, 2, \dots, M\}$  in a log-log plot. The R/S statistic still linearly increases with increases in

the length of series  $n$  in a log-log plot. Compared to the slopes in the middle of Figs. 4a and b, the slope estimated from the derived wireless cellular coverage boundary is clearly less than the slope estimated from the measured wireless cellular coverage boundary in log-log plots. Utilizing a least squares method, the Hurst parameter (i.e., the rate of increase of the R/S statistic) is estimated to be  $H = 0.5011 \approx 0.5$ . On the right of Fig. 4b, the variance-time analysis method is used to estimate the value of the Hurst parameter via the variance of aggregated series of the random process  $X' = \{\phi'_i, i = 1, 2, \dots, M\}$ . The variance of aggregated series presents a linear decaying characteristic with increases in the aggregation level  $m$  in a log-log plot. Utilizing a least squares method, the slope of sample variances is estimated to be  $\beta = 0.9690$  in the log-log plot. Furthermore, the value of the Hurst parameter is calculated to be  $H = 1 - (\beta/2) = 0.5155 \approx 0.5$ . Based on the results from the three Hurst parameter estimators, the value of the Hurst parameter estimated from the derived wireless cellular coverage boundary is  $H \approx 0.5$ .

Compared to the values of the Hurst parameter in Table 2, the values of the Hurst parameter estimated from the measured wireless cellular coverage boundary is located in the interval (0.5, 1.0) (i.e.,  $H \approx 0.9$ ). Therefore, the measured wireless cellular coverage boundary has the statistical fractal characteristic in angular scales.

Although the measured wireless cellular data in this study is collected from the Pingjiang Road, Shanghai China, the measurement location was not specially selected for the evaluation of the wireless cellular coverage boundary. Obstacles around the BS are distributed by city planning, and no specified changes have been forced on the obstacles in the measurement process. Moreover, the measurement route includes the wireless signal propagation fading shaded by office buildings and green belts in urban scenarios. Despite the slight deviation of the Hurst parameter values estimated by the three typical methods, the final estimated result of the measured wireless cellular coverage boundary can be considered as consistent, that is, the value of Hurst parameter is  $H \approx 0.9$ , considering the system error generated by estimators themselves. In addition, we also analyze other measured wireless cellular data from Pingjiang Road on May 23, 2014 and the

Hurst parameter estimation method	Hurst parameter	
	Measured wireless cellular coverage boundary	Derived wireless cellular coverage boundary
Periodogram method	0.9013	0.4995
Rescaled adjusted range statistic method	0.9000	0.5011
Variance-time analysis method	0.8898	0.5155

Table 2. Hurst parameter of the wireless cellular coverage boundary.

other two BSs located in the urban and suburban areas of Shanghai, China. The detailed analysis results are illustrated in Table 3. The analysis results from all of the measured wireless cellular data indicate that the mean values of the Hurst parameter estimated from the measured wireless cellular coverage boundaries approximate 0.9. Therefore, the analysis result in this article is reasonable, and the real wireless cellular coverage boundary has the statistical fractal characteristic.

## CONCLUSIONS

Considering the anisotropy fading of wireless signal propagated in non-free spaces, the statistical characteristics of the wireless cellular coverage boundary have been measured and analyzed in this article. The analyzed results indicate that the measured wireless cellular coverage boundary is extremely irregular, and it is difficult to depict the measured wireless cellular coverage boundary using conventional Euclidean geometry methods. Thus, based on fractal geometry theory, the statistical characteristic of the measured wireless cellular coverage boundary was estimated using three typical Hurst parameter estimators. Our results validate the fact that the real wireless cellular coverage boundary has the statistical fractal characteristic in angular scales. Therefore, real wireless cellular networks can be called wireless fractal cellular networks.

By utilizing fractal geometric theory, random processes that exhibit the fractal characteristic have been put forward to fit wireless fractal cel-

Hurst parameter estimation method	Hurst parameter		
	Zhangjiang Road, Shanghai, China. April 22, 2014	Pingjiang Road, Shanghai, China. May 23, 2014	Tianshan Road, Shanghai, China. June 4, 2014
Periodogram method	0.9188	0.9120	0.9096
Rescaled adjusted range statistic method	0.9313	0.9420	0.9020
Variance-time analysis method	0.8865	0.8673	0.9252
Mean value of Hurst	0.9122	0.9071	0.9096

Table 3. Hurst parameters of the other three measured cellular coverage areas.

Our results validate the fact that the real wireless cellular coverage boundary has the statistical fractal characteristic in angular scales. Therefore, real wireless cellular networks can be called wireless fractal wireless cellular networks.

lular networks. Therefore, based on the fractal characteristic validated in this article, a new system model of cellular networks could be built to analyze and optimize the performance of random cellular networks in the following areas.

**Improving Cooperative Transmission Efficiency:** Based on our measured data, the distance between the wireless cellular coverage boundary and the associated BS is more than 180 km in specified directions. In this case, the new cooperative transmission scheme needs to include non-adjacent cooperative BSs located at remote regions and further improve the transmission efficiency considering direction effects among the user and cooperative BSs.

**Optimizing Energy Efficiency:** Green communication is an important topic for future cellular networks. Based on results in this article, a fractal wireless cellular coverage model can be expected to describe the wireless cellular coverage areas. Furthermore, the optimal energy efficiency of cellular networks can be achieved by adjusting the BS transmission power considering wireless fractal cellular coverage areas.

**Beamforming Technologies:** Based on the beamforming technologies, new angular power control technologies can be developed to improve the transmission efficiency and energy efficiency of cellular networks. Different from conventional power control technologies, which adjust the BS transmission power based on the channel state information, the new angular power control technologies can adaptively adjust the transmission power in different directions considering the fractal characteristic of wireless cellular coverage boundary.

### ACKNOWLEDGMENTS

The corresponding authors of the article are Prof. Xiaohu Ge and Yang Yang. The authors would like to acknowledge the support from the International Science and Technology Cooperation Program of China (Grant No. 2014DFA11640, 2015DFG12580, and 2014DFE10160), the National Natural Science Foundation of China (NSFC) (Grant No. 61231009 and 61461136003), the NSFC Major International Joint Research Project (Grant No. 61210002), the China 863 Project (Grant No. 2014AA01A701 and 2014AA01A707), the Science and Technology Commission of Shanghai Municipality (STCSM) under grant 14ZR1439700, the Fundamental Research Funds for the Central Universities (Grant No. 2015XJGH011), EU FP7-PEOPLE-IRSES (Contract/Grant No. 247083, 318992, 612652 and 610524), the EPSRC TOUCAN project (Grant No. EP/L020009/1), and EU H2020 ITN 5G Wireless project (Grant No. 641985).

### REFERENCES

- [1] C. Stephen et al., "Ericsson Mobility Report," tech. rep., June 2015; <http://www.ericsson.com/news/1925907>.
- [2] M. Chen et al., "On The Computation Offloading at Ad Hoc Cloudlet: Architecture and Service Models," *IEEE Commun. Mag.*, vol. 53, no. 6, June 2015, pp. 18–24.
- [3] J. G. Andrews, F. Baccelli, and R. K. Ganti, "A New Tractable Model for Cellular Coverage," *IEEE Trans. Wireless Commun.*, vol. 59, Sept. 2011, pp. 1204–11.
- [4] F. Baccelli et al., "Stochastic Geometry and Architecture of Communication Networks," *J. Telecommun. Sys.*, vol. 7, no. 1, June 1997, pp. 209–27.

- [5] A. J. Goldsmith and L. J. Greenstein, "A Measurement-Based Model for Predicting Coverage Areas of Urban Microcells," *IEEE JSAC*, vol. 11, no. 7, Sept. 1993, pp. 1013–23.
- [6] M. Haenggi and R. K. Ganti, "Interference in Large Wireless Networks," *Foundations and Trends in Networking*, vol. 3, no. 2, 2008, pp. 127–248.
- [7] N. Liliith and K. Dogancay, "Using Reinforcement Learning for Call Admission Control in Cellular Environments Featuring Self-Similar Traffic," *IEEE TENCON.*, 2005, pp. 1–6.
- [8] B. B. Mandelbrot, *The Fractal Geometry of Nature*, 1982.
- [9] B. B. Mandelbrot, "Long-Run Linearity, Locally Gaussian Processes, H-Spectra and Infinite Variances," *Int'l. Econ. Rev.*, vol. 10, no. 1, Feb. 1969, pp. 82–113.
- [10] H. E. Hurst, R. P. Black, and Y. M. Simaika, *Long-Term Storage: An Experimental Study*, 1965.
- [11] V. Erceg et al., "An Empirically Based Path Loss Model for Wireless Channels in Suburban Environments," *IEEE JSAC*, vol. 17, no. 7, July 1999, pp. 1205–11.
- [12] W. C. Y. Lee, "Estimate of Local Average Power of a Mobile Radio Signal," *IEEE Trans. Vehic. Tech.*, vol. 34, no. 1, Feb. 1985, pp. 22–27.
- [13] X. Ge et al., "Spatial Spectrum and Energy Efficiency of Random Cellular Networks," *IEEE Trans. Commun.*, vol. 63, no. 3, Mar. 2015, pp. 1019–30.
- [14] W. Jakes, *Microwave Mobile Communications*, 1974.
- [15] W. E. Leland et al., "On the Self-Similar Nature of Ethernet Traffic (extended version)," *IEEE/ACM Trans. Net.*, vol. 2, no. 1, Feb. 1994, pp. 1–15.
- [16] S. Mordechai, S. Marin, and J. M. Dudley, "Fractal Optics and Beyond," *Nat. Photon.*, vol. 6, Mar. 2012, pp. 209–10.
- [17] X. Ge, G. Zhu, and Y. Zhu, "On the Testing for Alpha-Stable Distributions of Network Traffic," *Comp. Commun.*, vol. 27, no. 5, Mar. 2004, pp. 447–57.

### BIOGRAPHIES

XIAOHU GE [M'09, SM'11] is currently a full professor with the School of Electronic Information and Communications at Huazhong University of Science and Technology (HUST), China, and an adjunct professor with the Faculty of Engineering and Information Technology at the University of Technology Sydney, Australia. He received his Ph.D. degree in communication and information engineering from HUST in 2003. He is the director of the China International Joint Research Center of Green Communications and Networking. He has been actively involved in organizing more than 10 international conferences since 2005. He served as General Chair for the 2015 IEEE International Conference on Green Computing and Communications. He serves as an Associate Editor for *IEEE Access*, the *Wireless Communications and Mobile Computing Journal* (Wiley), and the *International Journal of Communication*.

YEHONG QIU received her B.E. degrees in communication engineering from HUST in 2014. She is currently working toward a Master's degree in the School of Electronic Information and Communications at HUST. Her research interests mainly include characteristic and performance analysis of wireless fractal cellular networks, and energy efficiency of wireless cellular networks.

JIAQI CHEN received her B.E. degree in communication engineering from HUST in 2013. She is currently working toward her Ph.D. degree at HUST. Her research interests include energy efficiency, fractal cellular networks, and handover.

MEIDONG HUANG received his B.E. degree in communication engineering from HUST in 2015. Now he is working toward his Master's degree at HUST. His research interests are mainly in cellular boundary analysis.

HUI XU received his B.Eng. and M.Eng. degrees in communication engineering from Shanghai Jiaotong University, P.R. China, in 2004. He is currently a senior engineer with the Shanghai Institute of Microsystem and Information Technology (SIMIT), Chinese Academy of Sciences (CAS), serving as the department head of the CAS Key Laboratory of Wireless Sensor Network and Communication, and the department head of the Shanghai Research Center for Wireless Communications (WiCO). Prior to that, he served the Department of Global Telecom Solutions at Motorola (China) Co., Ltd, as an R&D senior engineer, and the Department of Production Quality at Shanghai Datang Telcom, China, as an R&D engineer. His research interests include wireless com-

---

munication networks, software defined wireless networks, 5G mobile systems, intelligent transport systems, wireless testbed development, and practical experiments.

JING XU received his M.S. degree in electronic engineering from Jilin University, Chang Chun, China, in 2001 and his Ph.D. degree from the Radio Engineering Department of Southeast University, Nan Jing, China, in 2005. He is a professor with SIMIT, CAS, and obtained a Shanghai Young Rising Star award (2010). His main research interests include inter-cell interference mitigation, interference modeling, cooperative communications, and software defined wireless networks.

Wuxiong Zhang received his B.E. degree in information security from Shanghai Jiao Tong University in 2008 and his Ph.D. degree in communication and information systems from SIMIT, CAS in 2013. He is currently an assistant professor at SIMIT, and serving as an assistant researcher at the Shanghai Research Center for Wireless Communications. His research interests include 4G/5G mobile communication systems and vehicular

YANG YANG [S'99, M'02, SM'10] received his B.Eng. and M.Eng. degrees in radio engineering from Southeast University in 1996 and 1999, respectively, and his Ph.D. degree in information engineering from the Chinese University of Hong Kong in 2002. He is currently a professor at SIMIT, CAS, serving as the director of the CAS Key Laboratory of Wireless Sensor Network and Communication, and the director of WiCO. He is also an adjunct professor with the School of Information Science and Technology, ShanghaiTech University. Prior to that, he served the Department of Electronic and Electrical Engineering at University College London, United Kingdom, as a senior lecturer; the Department of Electronic and Computer Engineering at Brunel University, United Kingdom, as a lecturer; and the Department of Information Engineering at the Chinese University of Hong Kong as an assistant professor. His research interests include wireless ad hoc and sensor networks, software

defined wireless networks, 5G mobile systems, intelligent transport systems, wireless testbed development, and practical experiments. He has co-edited a book on heterogeneous cellular networks (2013, Cambridge University Press) and co-authored more than 100 technical papers. He has served on the organization teams of about 50 international conferences.

CHENG-XIANG WANG [S'01, M'05, SM'08] received his Ph.D. degree from Aalborg University, Denmark, in 2004. He has been with Heriot-Watt University since 2005 and became a professor in 2011. His research interests include wireless channel modeling and 5G wireless communication networks. He has served or is serving as an Editor or Guest Editor for 11 international journals, including *IEEE Transactions on Vehicular Technology* (2011–), *IEEE Transactions on Communications* (2015–), *IEEE Transactions on Wireless Communications* (2007–2009), and the *IEEE Journal on Selected Areas in Communications*. He has published one book and over 240 papers in journals and conferences.

JOHN THOMPSON [M'03, SM'12, F'16] is currently a professor in signal processing and communications at the School of Engineering, University of Edinburgh. He specializes in antenna array processing, cooperative communications systems, and energy-efficient wireless communications. He has published in excess of 300 papers on these topics, including 100 journal paper publications. He is currently the project coordinator for the EU Marie Curie International Training Network project ADVANTAGE studying smart grid technology and for the EPSRC SERAN research project which investigates concepts for fifth generation wireless systems. He was recently a Distinguished Lecturer for the IEEE in the field of Green Communications (2014–2015). He is an Editor for the Green Communications and Computing Series that appears regularly in *IEEE Communications Magazine*. In January 2016, he was elevated to Fellow of the IEEE for contributions to multiple antenna and multihop wireless communications.